Atmospheric Research 315 (2025) 107872

Contents lists available at ScienceDirect

Atmospheric Research

journal homepage: www.elsevier.com/locate/atmosres

Major May tornado outbreaks in the United States: Novel multiscale atmospheric patterns identified using maximum covariance analysis

Paulina Ćwik[a,b,*], Jason C. Furtado[c], Renee A. McPherson[a,b], Mateusz Taszarek[d]

[a] Department of Geography and Environmental Sustainability, The University of Oklahoma, 100 E Boyd St, Suite 510, Norman, OK, United States of America
[b] South Central Climate Adaptation Science Center, 201 Stephenson Parkway, Suite 2100, Norman, OK, United States of America
[c] School of Meteorology, The University of Oklahoma, 120 David L. Boren Blvd, Suite 5900, Norman, OK, United States of America
[d] Department of Meteorology and Climatology, Adam Mickiewicz University in Poznań, Poland

ARTICLE INFO

Keywords:
Tornado outbreaks
Atmospheric patterns
Statistical analysis
Maximum covariance analysis
ERA-5
500-hPa geopotential height anomalies
WMAXSHEAR anomalies

ABSTRACT

This study investigates the atmospheric conditions associated with major tornado outbreaks (at least seven tornadoes of magnitude EF2 or higher) in the United States during May using maximum covariance analysis (MCA). We focus on identifying the leading modes of covariability between 500-hPa geopotential height anomalies and the WMAXSHEAR parameter, a bivariate proxy of atmospheric buoyancy and vertical wind shear. By analyzing 91 significant tornado outbreaks from 1950 to 2019, we identify three primary multivariate patterns, each exhibiting distinct anomaly locations and intensities for both variables. These patterns account for 97 % of the covariability between the two fields, with the leading pattern (MCA1) explaining 71 %, the second (MCA2) 20 %, and the third (MCA3) 6 %. The application of MCA to tornado outbreak analysis is a novel approach, providing a nuanced understanding of the complex multi-scale atmospheric conditions leading to these events.

We find that tornado outbreaks associated with the first two leading covariability patterns last longer ad can occur at any time of day and night, whereas those associated with the third pattern tend to be shorter and begin in the late morning or early evening. The identified patterns are significantly different from those observed on null-event days, suggesting that these patterns are useful for future research aimed at simulating and comparing tornado outbreak characteristics under scenarios of a warming climate. This research enhances our understanding of the complex interplay between mesoscale and synoptic-scale atmospheric conditions and provides valuable insights for improving tornado outbreak predictions and preparedness in a changing climate.

1. Introduction

Many studies have addressed the relationship between severe thunderstorms capable of producing tornadoes or tornado outbreaks and associated environmental variables (e.g., Brooks et al., 2003a; Thompson et al., 2012; Lee et al., 2013; Coniglio and Parker, 2020; Bagaglini et al., 2021; Pilguj et al., 2022a). This multi-decadal research interest emerged because tornadic storms are among the most devastating natural phenomena, and while local, they cause immense social and material impacts (e.g., Simmons et al., 2013; Allen and Allen, 2016; Strader et al., 2016; Antonescu et al., 2017; Hatzis et al., 2020; Anderson-Frey and Brooks, 2021; Púčik et al., 2024). As global average temperatures increase due to anthropogenic forcing (Masson-Delmotte et al., 2021), changes to the environments favorable to the development of tornado outbreaks have been observed. For example, in the United States, Tippett (2014) reported an increase in tornado reports after 2000, alongside a heightened volatility of environments favorable to tornado formation. Other studies have documented a relationship between an increased number of tornadoes per tornado outbreak, defined as, for example, a sequence of at least six tornadoes of EF1 or greater intensity in close succession (as in Fuhrmann et al., 2014), and increasing trends in wind, moisture, and atmospheric instability observed over time (Schroder and Elsner, 2020; Moore et al., 2021). Changing climate conditions may alter favorable tornadic environments (Strader et al., 2017; Ashley et al., 2023) and contribute to changes in the frequency and spatiotemporal characteristics of tornadic storms in the future, which is of great concern

* Corresponding author at: Department of Geography and Environmental Sustainability, The University of Oklahoma, 100 E Boyd St, Suite 510, Norman, OK, United States of America.
E-mail address: paulinacwik.new@gmail.com (P. Ćwik).

https://doi.org/10.1016/j.atmosres.2024.107872
Received 27 July 2024; Received in revised form 2 December 2024; Accepted 14 December 2024
Available online 17 December 2024
0169-8095/

to communities, policy officials, emergency managers, and researchers (Klockow et al., 2014; Rothfusz et al., 2018). Historical changes in tornadic environments provide a context to better understand the role of anthropogenic climate change in modulating tornado outbreak characteristics during the present and in the future. Recent observations indicate increased tornado activity in regions east of 'Tornado Alley' (Moore and DeBoer, 2019) and during winter months in the Southeast US (Gensini and Brooks, 2018; Molina and Allen, 2020; Taszarek et al., 2021a), though it remains uncertain whether these trends represent a long-term shift or inherent short-term variability.

Important conditions for severe storm development include: (1) sufficient atmospheric instability, (2) strong vertical wind shear, (3) abundant moisture in the boundary layer, and (4) an initiating mechanism to trigger deep moist convection, e.g., an orographic feature, frontal system, dryline, or low-level convergence zone (Rasmussen, 2003; Thompson et al., 2004; Mercer et al., 2012; Sherburn and Parker, 2014). Tornadic thunderstorms that evolve from supercells (Markowski and Richardson, 2010; Davies-Jones, 2015) are more likely to form in environments characterized by high values of convective available potential energy (CAPE; Thompson et al., 2003), which represents the amount of buoyancy in the troposphere necessary to fuel a storm's updraft (Johns and Doswell III, 1992; Rasmussen and Blanchard, 1998). However, CAPE itself is a poor predictor of tornadoes because even substantial instability will not result in a tornado if sufficient vertical wind shear is absent. Tornadoes are also supported by strong 0–6 km wind shear (>25 m s^{-1}, S06 hereafter), which refers to the magnitude difference between the wind speeds at the surface and 6 km above the ground. S06 controls the organization of mid-level rotation and supports the formation of long-lived supercells (Brooks et al., 2003b; Coffer et al., 2019). In addition to the mesoscale atmospheric ingredients, most tornado outbreaks are forced by large-scale features, such as upper-level troughs (Corfidi et al., 2010; Brown and Nowotarski, 2020; Chasteen and Koch, 2022), and there is a recognition that distinct, synoptic-scale patterns in 500-hPa geopotential heights are associated with enhanced potential for tornado outbreaks (Sparrow and Mercer, 2016; Gensini et al., 2019). Recently, Ćwik et al. (2022) identified three synoptic-scale patterns in mid-tropospheric geopotential height anomalies associated with historic tornado outbreaks in the US in May. Two of these patterns were identified as representative of historic May tornado outbreaks. The combination of favorable thermodynamic and kinematic environments is a primary reason why most tornadoes occur in mid-latitudes, where both factors are often present. Our work extends the research of Ćwik et al. (2022) to include a variable that affects the mesoscale environment, combines thermodynamic and kinematic features, and is of key importance to the development of tornado outbreaks.

This study's goal is to demonstrate a statistical method that identifies meteorological patterns that are evident on various atmospheric scales and associated with tornado outbreaks. Usually, both the mesoscale environment and large-scale forcing support tornado outbreaks. To study these multi-scale environments, we apply multivariate statistics (as opposed to the univariate approach in Ćwik et al., 2022). We specifically analyze the modes of covariability between 500-hPa geopotential height anomalies and the anomalous WMAXSHEAR parameter, which combines instability (CAPE) and deep-layer shear (S06) (Brooks, 2013; Taszarek et al., 2020). This analysis focuses on days linked to historic major May tornado outbreaks, defined as events with seven or more tornadoes rated EF2 or higher on the Enhanced Fujita scale (Ćwik et al., 2022), occurring between 1950 and 2019 east of the Rocky Mountains in the US. The selection of May was based on its distinction as the month with the highest frequency of major tornado outbreaks (Fuhrmann et al., 2014; Ćwik et al., 2022). This decision was intentional to avoid influence of seasonal fluctuations and to allow for comparisons with the methodology employed in previous research by Ćwik et al. (2022). Previously, Taszarek et al. (2020) noted that environments characterized by high values of WMAXSHEAR have a higher potential for tornadoes to become significant (i.e., EF2 or greater) and, thus, a higher likelihood for a major tornado outbreak, as defined by Ćwik et al. (2022). Considering the interdependency of tornado outbreak ingredients occurring on multiple spatial scales, we hypothesize that there are specific modes of covariability of these two fields (500-hPa geopotential height anomalies and WMAXSHEAR) that are tied to tornado outbreaks occurring in the eastern US. We will test this hypothesis using maximum covariance analysis (MCA; Prohaska, 1976). By exploring the modes of covariability between anomalies of 500-hPa geopotential height and WMAXSHEAR, we aim to deepen our understanding of the complex interplay between atmospheric conditions and tornado outbreaks in the US. Unraveling these relationships not only enhances our knowledge of severe weather phenomena but also holds implications for comparison with simulations of future changes to tornado outbreak characteristics.

2. Data and methods

2.1. Tornado outbreaks

For the purpose of this work, only significant tornadoes i.e., EF2 or greater on the (Enhanced) Fujita scale (Doswell et al., 2006; Edwards et al., 2021), were included, as they result in the majority of tornado-related deaths and are less susceptible to population biases in reporting (Elsner et al., 2013; Groenemeijer and Kühne, 2014). There are many diverse "tornado outbreak" definitions that evolved over the years (Ćwik et al., 2021). Herein, we used the technique from Shafer and Doswell (2011) where tornado reports were grouped in 24-h clusters within a constrained region using kernel density estimation (KDE; Silverman, 1986; Anderson-Frey et al., 2016). Additionally, like Ćwik et al. (2022), we applied a threshold of seven or more significant tornadoes per tornado outbreak (major tornado outbreak) and used a smoothing parameter h = 1 with a PDF threshold probability of 0.001 (Shafer and Doswell, 2011) to calculate the specific geographic region for each outbreak. This method resulted in a database of 341 major tornado outbreaks that occurred across the US from 1950 to 2019. However, in this work, we focus only on outbreaks occurring during May (n = 91; Fig. 1), with their specific dates detailed in Ćwik et al., 2022.

In the US, atmospheric conditions that favor tornado formation, such as favorable overlap of strong vertical wind shear with sufficient thermodynamic instability, occur with greatest frequency east of the Rocky Mountains (Galway, 1977; Gensini and de Guenni, 2019). Consequently,

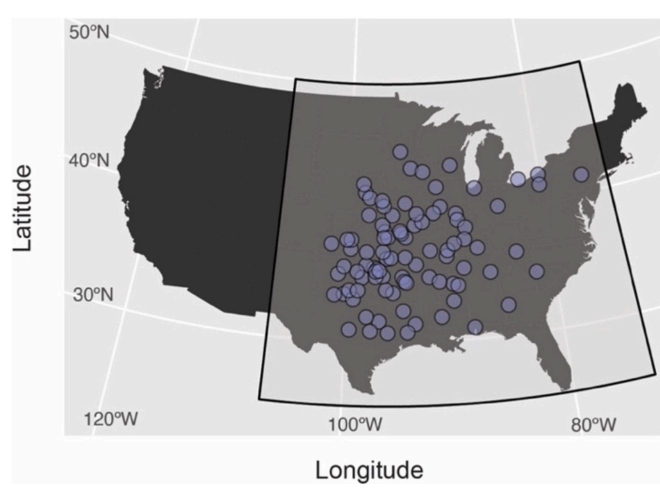

Fig. 1. Spatial distribution of centroids (purple circles) of 91 major tornado outbreaks during May from 1950 to 2019, based on KDE analysis. Spatial domain extent is 50°N, 106°W to 25°N, 70°W (black-framed region) and is used in this study for pattern identification. (For interpretation of the references to colour in this figure legend, the reader is referred to the web version of this article.)

most tornado outbreaks are observed in the region extending from ~106°W to the US East Coast (Mercer and Bates, 2019). Therefore, we conducted a spatiotemporal analysis of the atmospheric patterns associated with major tornado outbreaks from 25 to 50°N and 70–106°W (Fig. 1, black outline). Centroids of major tornado outbreaks (circles in Fig. 1) were calculated as the arithmetic mean position based on the tornado reports database from the Storm Prediction Center (SPC) of the National Oceanic and Atmospheric Administration's (NOAA) National Weather Service (NWS) (Schaefer and Edwards, 1999).

2.2. Reanalysis

Reanalysis datasets are commonly used to investigate atmospheric environments, and several different reanalyses have been used in studying climatologies of severe convective weather (Gensini et al., 2014; Tochimoto and Niino, 2016; King and Kennedy, 2019). In our work, we applied the 5th version of European Centre for Medium-Range Weather Forecasts reanalysis (ERA5; Hersbach et al., 2020). Although ERA5 is considered to be one of the most reliable available reanalysis datasets, it is not free of biases. As found by Li, and D.R., C., Reed, K. A., Dawson, D. T. (2020), Taszarek et al. (2021b), and Pilguj et al. (2022b), ERA5 tends to underestimate extreme CAPE environments, while providing reliable estimates of S06 with only a minor underestimation. As a result, WMAXSHEAR tends to be slightly underestimated, especially for extreme values, but, as noted by the same authors, these biases are not significant and, overall, ERA5 reproduces severe local storm environments across the US reasonably well. In addition, WMAXSHEAR does not depend on knowing storm motion, unlike Storm-Relative Environmental Helicity or Significant Tornado Parameter, and therefore it is better represented in ERA5 than other, more complex parameters (Thompson et al., 2003; Taszarek et al., 2021b). Furthermore, because of strong spatiotemporal correlation of ERA5 with observational data (Taszarek et al., 2021b) and hourly output that offers more faithful representation of the mesoscale environments (compared to e.g., 6-hourly outputs in other reanalyses), ERA5 was deemed sufficient for purposes of this work.

Building on the methodology of Ćwik et al. (2022), for each major tornado outbreak in May, we extracted the 500-hPa geopotential height field from ERA5 at the earliest time available before or at the onset of the outbreak. We computed hourly anomalies in the 500-hPa geopotential height and WMAXSHEAR at each grid point by subtracting the hourly climatology value from the hourly values, using a reference period from 1991 to 2020. This calculation involved using mixed-layer CAPE and S06 at each grid point, date, and time (Eq. 1):

$$\mathrm{WMAXSHEAR} = \sqrt{2^{*}\mathrm{CAPE}}^{*}\mathrm{S06} \tag{1}$$

where CAPE and S06 were derived from 137 raw hybrid-sigma model levels of temperature, specific humidity, u- and v- wind components, geopotential height, and pressure, using 'thundeR' R-language rawinsonde package (Taszarek et al., 2023; Czernecki et al., 2023). For CAPE calculations, we used a 0–500 m mixed-layer parcel.

We applied MCA to study the multivariate relationship between WMAXSHEAR anomalies (denoted by **X**) and 500-hPa geopotential height anomalies (denoted by **Y**). MCA assesses the overall covariability between two sets of variables instead of focusing solely on the variability of one. This technique provides an advantage by enabling detailed spatial identification of patterns associated with tornado outbreaks in a variety of environments. Consequently, the patterns derived from MCA support better understanding of the timing, duration, and location of major tornado outbreaks.

Before executing MCA, data were linear detrended at each grid point. To mitigate the effects of autocorrelation, we filtered the dataset to include only the 1900 UTC measurements for every day in May, aligning with the typical peak of major tornado outbreak initiations. To adjust for variations in grid area at different latitudes, these detrended values were weighted by the square root of the cosine of latitude. The dispersion matrix is:

$$\mathbf{C} = \frac{1}{M}\mathbf{X}^{T}\mathbf{Y} \tag{2}$$

where **C** is the covariance matrix, M is the shared time dimension, and T represents the transpose operator. We applied singular value decomposition to **C** to find the leading modes of covariability between the fields. The variance explained by each covariability mode, k, was calculated using squared covariance fraction (SCF):

$$\mathrm{SCF} = \frac{\sigma_k^2}{\sum_{k=1}^{K}\sigma_k^2} \tag{3}$$

where σ_k is the singular value for mode k and K is the total number of singular values (i.e., number of covariability modes found). To check if both fields are well correlated enough for MCA, we used the root mean squared covariance (RMSC):

$$\mathrm{RMSC} = \left[\frac{\sum_{i=1}^{N}\sum_{j=1}^{P}\left(\overline{x_i y_j}\right)^2}{\sum_{i=1}^{N}\overline{x_i^2}\sum_{j=1}^{P}\overline{y_j^2}}\right]^{\frac{1}{2}} \tag{4}$$

where N and P represent spatial dimensions of **X** and **Y,** and x_i and y_j are individual elements of **X** and **Y**. Typically, RMSC values of ≥0.1 are considered meaningful, signifying a strong correlation between fields **X** and **Y** suitable for conducting MCA (Hartmann, 2016). This RMSC constraint ensures that the variables exhibit a robust correlation, establishing a reliable foundation for subsequent MCA. In our analysis, RMSC = 0.3.

The patterns resulting from MCA are presented as homogeneous regression maps, where each field (unweighted anomalies) is regressed onto its respective time series of standardized expansion coefficients (EC). To assess potential changes in the EC time series over time, we employed permutation testing with 1000 rearrangements. This method evaluates whether deviations in group means contradict the null hypothesis of no significant decadal variations. By shuffling data labels and preserving the data's distribution, this approach establishes a statistical reference independent of distribution assumptions.

Finally, to determine whether the MCA patterns identified in this study differ from those observed on days without major tornado outbreaks (i.e., "null-event days"), we isolated all such days from our dataset. It is important to note that these null-event days, as per our definition, may still include tornado occurrences but do not meet the number and intensity threshold set for our major tornado outbreaks. We applied MCA to this null-event subset using only data from 1900 UTC. Next, we assessed the statistical significance of differences between the major tornado outbreak patterns and null-event patters by employing a bootstrap test whereby we resampled the datasets 1000 times with replacement for data only at grid points with negative 500-hPa geopotential height anomalies. This approach is designed to account for the variability and ensure robust comparisons between the two groups by generating multiple resampled datasets to create an empirical distribution of the statistic of interest. The bootstrap technique is widely used in atmospheric and climate sciences to assess the reliability of statistical estimates (e.g., Marchand et al., 2006; Wilks, 2011; Gilleland, 2020).

3. Results

Fig. 2 illustrates the first three leading modes of covariability—hereafter MCA1, MCA2, and MCA3—between May 500-hPa geopotential height anomalies and WXMAXSHEAR on major tornado outbreak days. These covariability modes account for 71 %, 20 %, and 6 %, of the covariance, respectively, and are depicted through homogeneous regression maps, showing unweighted anomaly fields regressed

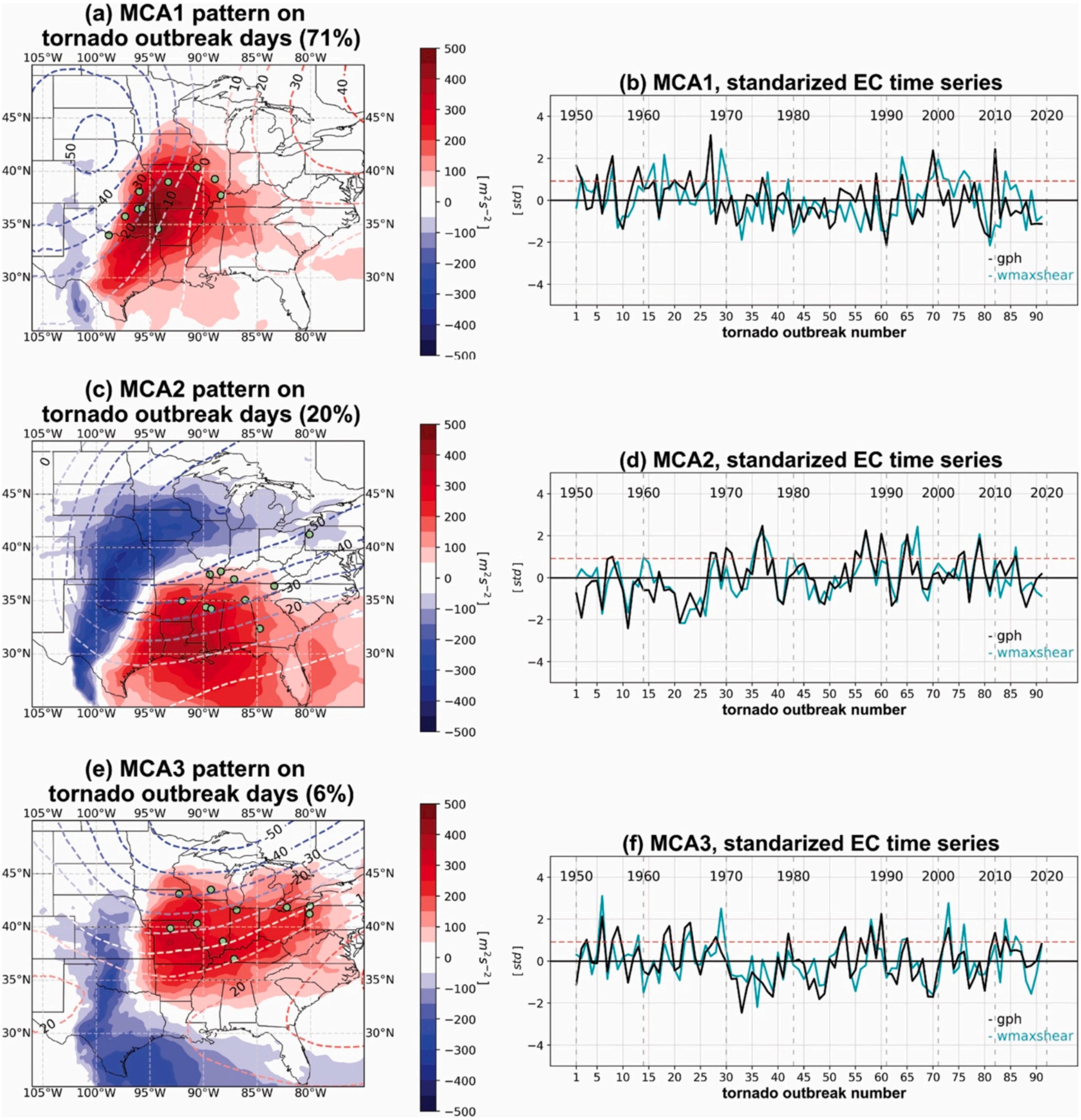

Fig. 2. (a) (shading) Regression of May WMAXSHEAR anomalies (interval of 50 m^2s^{-2}) onto the leading standardized WMAXSHEAR expansion coefficient (EC) time series from MCA (see text); (dashed contours) regression of May 500-hPa geopotential height anomalies (interval of 10 m) onto the 500-hPa geopotential height standardized EC; and (green dots) the centroids of 10 major tornado outbreaks representative of the depicted pattern. Covariance explained by the mode listed in parenthesis in the title. (b) The standardized EC time series for anomalous WMAXSHEAR (green) and 500-hPa geopotential height (black) for MCA1. (c) As in (a) but for the second leading mode of covariability. (d) As in (b) but for MCA2. (e) As in (a) but for the third leading mode of covariability. (f) As in (b) but for MCA3.

onto the standardized time series of their ECs. We identified ten significant tornado outbreaks (marked as green dots) for each mode to demonstrate their geographic distribution relative to MCA patterns. These outbreaks were selected based on a threshold (represented by the red dashed line in Fig. 2b, 2d, 2f) designed to include a total of 10 cases for graphical visualization purposes only. All statistical analyses were conducted based on all 91 tornado outbreak cases. Fig. 3 presents examples of two selected tornado outbreaks associated with each of the three identified MCA patterns.

In the leading mode of covariability (MCA1, Fig. 2.2a), WMAXSHEAR anomalies are predominantly positive stretching from central Texas northward across the Plains into the Midwest. These anomalies peak over eastern Oklahoma, western Arkansas, and southwestern Missouri, reaching a maximum value of approximately 498 m^2s^{-2}. With sparse occurrence, the only region within MCA1 exhibiting relatively small (~ -130 m^2s^{-2}) negative WMAXSHEAR anomaly values, is

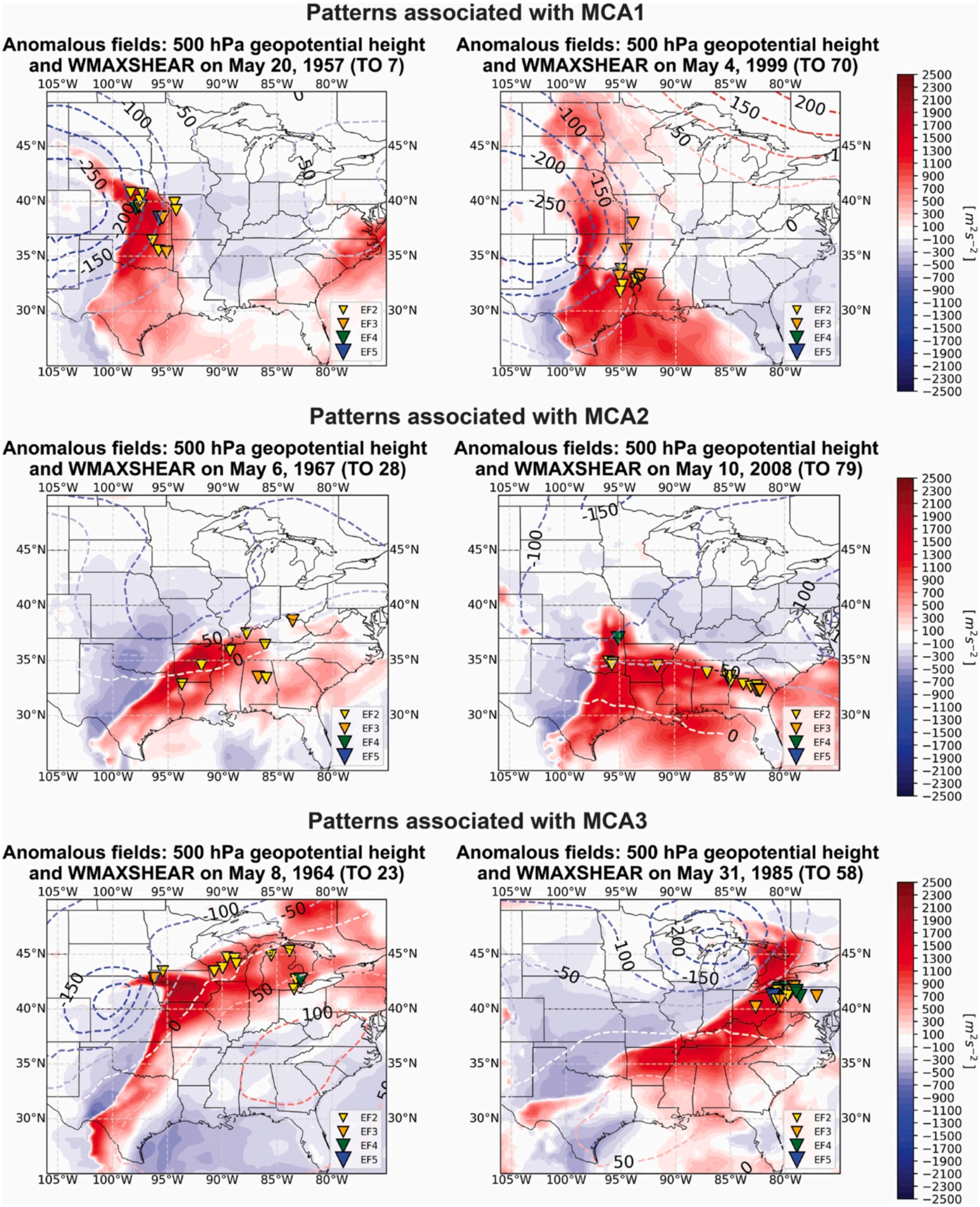

Fig. 3. Anomalous 500-hPa geopotential height (contours) and WMAXSHEAR (shading) fields for two representative tornado outbreaks for each MCA. Locations of EF2 or stronger tornadoes within each outbreak are marked with triangles. The numbers of selected tornado outbreaks (e.g., TO7 for the 7th outbreak in the record) are provided in the captions.

western Texas Panhandle region. The 500-hPa geopotential height anomalies depict lower-than-average heights over the western U.S. extending southward, with lowest values (−53 m) over South Dakota, and Nebraska. Simultaneously, positive anomalies occur over the northeastern US.

Results of the permutation tests (Table S1) for WMAXSHEAR anomalies in the MCA1 EC time series indicate statistically significant deviations, with *p*-values below 0.05, when comparing the 1980s and several other decades (1950s, 1960s, 1990s, and 2000s). These findings suggest interdecadal changes in the amplitude of WMAXSHEAR anomalies associated with MCA1. Specifically, the early 1980s displayed a consistent pattern expression that deviated minimally from the established MCA1, showing little variation in comparison to other periods. Similarly, the 500-hPa geopotential height anomalies in MCA1 show statistically significant differences for major tornado outbreaks in the 1980s when compared with those in earlier decades. Interestingly, the differences in amplitude observed in the EC time series of both variables during the 1980s coincide with decreased variability in the number of tornadoes per outbreak, particularly for the most severe EF4 and EF5 tornadoes (Fig. S1). Additional analysis (not shown) reveals that major tornado outbreaks with the largest number of events per occurrence (major tornado outbreak number 15 and 71, each with 25 tornadoes), and those that caused the most injuries and deaths (outbreak 29 with 1149 injured and outbreak 84 with 158 dead) are associated with the MCA1 pattern. Although this correspondence suggests a possible link, it does not imply causation between the MCA1 anomalies and the characteristics or specific impacts of these major tornado outbreaks.

MCA2 accounts for 20 % of the covariability between WMAXSHEAR anomalies and 500-hPa height anomalies (Fig. 2c). The spatial pattern of WMAXSHEAR anomalies features a northwest-to-southeast oriented dipole, with its center over the Oklahoma-Missouri border. The negative values extend from western Texas through Oklahoma and Kansas, and into the Upper Midwest, peaking at approximately $-382\ m^2s^{-2}$ over Oklahoma. A distinct region of positive WMAXSHEAR values dominates over the Mid-South, with the largest values ($\sim 405\ m^2s^{-2}$) across Louisiana. The dipole in anomalous WMAXSHEAR is spatially aligned with a pronounced (~ -60 m over), positively tilted longwave trough at 500 hPa centered over eastern Wisconsin and extending across Iowa, Missouri, and Kansas. The trough stretches south-southeastward, spanning nearly the entire domain as it extends over the Gulf of Mexico. Permutation test results (Table S1) on WMAXSHEAR anomalies in the MCA2 EC time series show significant differences particularly when comparing the 1960s to the 1990s and 2000s. Similarly, significant differences in 500-hPa geopotential height anomalies were observed when comparing the 1950s and 1960s against later decades (1970s, 1980s, and 2000s). Notably, the pattern expressions during the 1950s and 1960s were less like the patterns in MCA2. This lower-than-average pattern frequency might explain the absence of corresponding major tornado outbreaks that matched the MCA2 pattern until the late 1960s.

The last pattern, MCA3, explains 6 % of the covariance between the two fields (Fig. 2e). The 500-hPa geopotential height anomaly field shows a longwave trough centered north of Lake Superior (-57 m) and extending south-southwestward into eastern Kansas. Simultaneously, anomalous weak ridges exist over western New Mexico, the southeastern US Atlantic coast, and the southeastern US. In MCA3, the center of positive WMAXSHEAR anomalies ($359\ m^2s^{-2}$) dominates over the eastern two-thirds of the domain, maximizes across Missouri, and spreads through Illinois and the Ohio River Valley. Anomalously negative WMAXSHEAR anomalies span the western Gulf of Mexico, central Texas, Oklahoma, and Kansas, stretching northward into Nebraska. Statistically significant differences for WMAXSHEAR anomalies associated with MCA3 exist during the 1970s and 1990s compared to those in the 1950s. Additionally, differences in 500-hPa geopotential height anomalies were noted between the 1970s and other decades, specifically the 1950s, 1960s, 1980s, and 2010s. This deviation in pattern frequency is noticeable, yet it presents challenges in drawing extensive conclusions due to the infrequent occurrence of the MCA3 pattern. The sporadic nature of this pattern throughout the time series restricts a thorough understanding of its characteristics and potential impacts.

In examining the onset times of major tornado outbreaks, the initiation of outbreaks corresponding to MCA1 and MCA2 patterns occur at various times throughout the day (Fig. S2), suggesting the influence of large-scale atmospheric dynamics. This facet also was evident from the significant duration of these outbreaks, with MCA2-related events lasting up to 21 h and MCA1 up to 19 h (Fig. S3). Such extended durations suggest that these patterns are not solely reliant on diurnal thermal processes but may be sustained by persistent atmospheric conditions that exceed the typical daytime heating cycle. In contrast, MCA3-associated outbreaks are noticeably shorter, typically concluding within 10 h and initiating shortly before or around midday (Fig. S2). This midday initiation and the shorter duration of MCA3 outbreaks imply a stronger reliance on diurnal heating for atmospheric instability conducive to thunderstorm activity. As the sun's influence diminishes after peak heating hours, the energy necessary for maintaining these storms decreases, leading to their quicker dissipation as compared to the more sustained activity observed with MCA1 and MCA2 outbreaks. It is important to note that these observations are based on the available data, with 65 tornado outbreaks fitting the MCA1 pattern, 16 for MCA2, and only 10 for MCA3. Therefore, while the insights presented are valid within the scope of the data we have, they may not capture the entire picture. The limited number of MCA3 cases, in particular, suggests that our analysis may not fully represent the broader dynamics associated with these patterns. Future research with more extensive data could provide a more comprehensive understanding of these phenomena.

To investigate the potential relationship between the standardized EC time series and the number of tornadoes per tornado outbreak, we examined both 500-hPa geopotential height anomalies (Fig. S4) and WMAXSHEAR anomalies (Fig. S5) within the context of all MCA patterns. The Pearson correlation coefficients (Table S2) indicate a statistically significant, albeit weak, relationship for MCA1 WMAXSHEAR anomalies with EF2-EF5 tornado outbreak counts ($r = 0.257$, $p < 0.5$), while no other statistically significant correlations were observed. Visual inspection of the EC time series suggests no consistent connection between stronger EC values and the number of tornadoes per outbreak. EC peaks occur at various times, not necessarily aligning with outbreaks that include a higher number of tornadoes. However, a general reduction in signal during the early 1980s is evident in both variables, coinciding with a period of fewer tornadoes per outbreak, potentially indicating shared variability on broader temporal scales. These findings highlight the complexity of the relationship and suggest that further research is needed to fully understand the role of these atmospheric patterns in influencing tornado outbreak characteristics.

Finally, to confirm that the three patterns identified using days of major tornado outbreaks were not merely reflections of climatological patterns associated with days both with and without outbreaks, we compared our findings with those obtained from MCA analysis on all other days (i.e., null-event days). These results (Fig. 4b, d, f) indicate that while there is spatial overlap in patterns between major tornado outbreak and null-event days, the relationship between maximum WMAXSHEAR anomalies and the lowest 500-hPa geopotential height anomalies is notably stronger on major tornado outbreak days. Specifically, on these days, maximum WMAXSHEAR anomalies are not only closer spatially to the center of the anomalous trough but also exhibit greater intensity (reaching maximum values of $498\ m^2s^{-2}$ for MCA1, $405\ m^2s^{-2}$ for MCA2, and $359\ m^2s^{-2}$ for MCA3), forming a more concentrated and compact pattern compared to null-event days. In contrast, on null-event days, the maximum WMAXSHEAR anomalies are weaker ($292\ m^2s^{-2}$ for MCA1, $289\ m^2s^{-2}$ for MCA2, and $87\ m^2s^{-2}$ for MCA3) and positioned farther from the lowest 500-hPa geopotential height anomalies. The relationship between these variables is also less distinct across all three patterns as the contour lines are more spread out across the domain forming, in general, less intense anomaly.

Furthermore, the results of the bootstrap test reveal statistically significant differences between the mean differences of the two groups (tornado outbreaks vs. null-event days) at the 95 % confidence interval for the three patterns. Specifically, for MCA1, the mean difference is 56.82 with a 95 % confidence interval of [53.37, 60.47], indicating a robust distinction in the WMAXSHEAR anomalies associated with major tornado outbreaks. Similarly, for MCA2, the mean difference is 55.70 with a 95 % confidence interval of [52.19, 59.21], and for MCA3, the

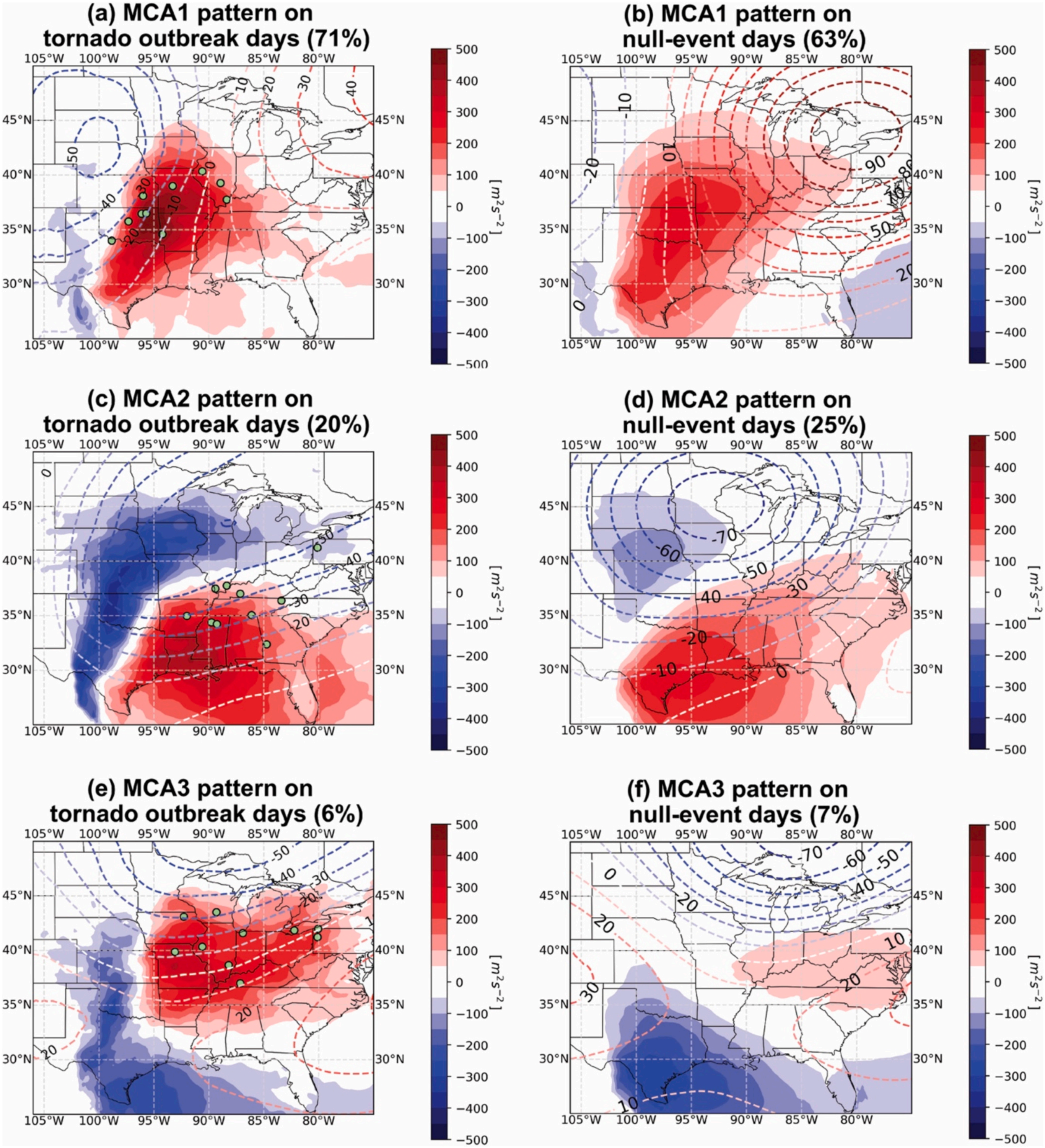

Fig. 4. Comparison of three MCA patterns on major tornado outbreak days (a, c, and e) and null-event days (b, d, and f) during May from 1950 to 2019.

mean difference is 45.67 with a 95 % confidence interval of [43.21, 48.13], underscoring the unique spatial pattern of atmospheric anomalies linked to major tornado outbreaks. The bootstrap analysis ensures that the observed differences are not due to random variability but reflect genuine distinctions in atmospheric conditions. Therefore, we conclude that the spatial patterns identified in association with major tornado outbreak days are significantly different from those observed on days without major tornado outbreaks, as defined in this study.

4. Discussion and conclusions

The primary goal of this work was to use maximum covariance analysis to identify dominant patterns of coupled variability between anomalies of WMAXSHEAR and anomalies of 500-hPa geopotential height associated with 91 major tornado outbreaks identified during Mays from 1950 to 2019. The three leading modes explained 71 %, 20 %, and 6 % of the covariability, respectively (97 % in total). For each mode, the center of positive WMAXSHEAR anomaly values was located to the south or southeast of an anomalous trough center in the 500-hPa geopotential height field. Prior studies indicate this alignment is dynamically and thermodynamically supportive of tornado outbreak development (Roebber et al., 2002; Corfidi et al., 2010; Molina et al., 2018). Patterns associated with tornado outbreak days were found to be significantly different from patterns on null-events days and, therefore, underscore the distinct atmospheric conditions associated with these two categories of days.

We identified significant interdecadal variations in the MCA patterns associated with major tornado outbreaks. MCA1 exhibited subdued activity during the 1980s, characterized by reduced amplitude variation in the EC time series and fewer tornadoes per outbreak, particularly in the most severe categories. Similarly, MCA2 showed a transition from subdued activity in the 1950s and 1960s to heightened occurrences in later decades, while MCA3, though less frequent, displayed notable disparities in the 1970s and 1990s compared to earlier periods. These interdecadal differences may result from factors such as decadal or longer-term variations in sea-surface temperatures, jet stream dynamics, and regional climate systems, as well as long-term anthropogenic influences on the climate, which could alter the frequency, intensity, and spatial distribution of conditions favorable for tornado outbreaks (e.g., Lee, 2012; Diffenbaugh et al., 2013; Elsner et al., 2015; Stendel et al., 2021). Previous studies (e.g., Gensini and Brooks, 2018; Molina and Allen, 2020) have documented a shift in tornado activity toward the southeastern United States in recent decades. While this study does not explicitly analyze spatial shifts, the observed interdecadal differences in MCA patterns highlight temporal variability in atmospheric environments that may help contextualize broader climatological trends and their influence on tornado activity. Further research is needed to investigate the mechanisms driving these changes and their potential connection to shifts in tornado occurrence.

In this work, we illustrated that MCA is an effective tool for reducing dimensionality of complex multivariate fields and identifying atmospheric patterns for severe weather episodes across the central and eastern United States. The advantage of the MCA as compared to a univariate approach (e.g., principal component analysis) is that it allows for more spatially detailed identification of patterns that are associated with tornado outbreaks in environments with forcings on different spatial scales (e.g., synoptic-scale 500-hPa geopotential height anomalies and mesoscale WMAXSHEAR anomalies). The MCA patterns identified in our analysis could potentially refine our predictions regarding the onset, duration, and likely areas affected by major tornado outbreaks. For example, the presence of the MCA1 pattern might signal a heightened risk of significant tornado activity across the eastern US Great Plains and western Greater Ozarks region. Notably, this pattern is not confined to a specific time of day, suggesting the possibility of prolonged and intense outbreaks when they do occur. Outbreaks corresponding to the MCA2 pattern are also likely to be long-lasting, with historic cases lasting up to 21 h, and can happen anytime of a day, with a pronounced impact expected in the US Southeast, a particularly vulnerable region of the nation with a high prevalence of mobile homes and limited tornado shelters (Sutter and Simmons, 2010; Fricker and Friesenhahn, 2022). In contrast, the MCA3 pattern is more commonly associated with major tornado outbreaks in the North-Central US and Northeast, with tornadoes beginning in the late morning and early afternoon but lasting for relatively short durations. Admittedly, the sample size of major tornado outbreaks corresponding to the MCA3 pattern is the smallest among the three, which necessitates cautious interpretation of these results.

Furthermore, these MCA patterns can be used as benchmarks for examining tornado outbreaks in global climate models. Specifically, tornadoes and tornado outbreaks occupy relatively small spatial scales that are not easily resolved by global climate models (Trapp et al., 2007; Trapp et al., 2009). Instead, a common practice is the use of environmental proxies that indicate favorable conditions supporting tornado occurrence (Diffenbaugh et al., 2013; Trapp and Hoogewind, 2016). The patterns presented herein were identified based on the environmental fields (i.e., CAPE, S06, and 500-hPa geopotential height) that are commonly used as proxies in research associated with tornadoes and tornado outbreaks (Tippett et al., 2016) also using global climate model simulations (Marsh et al., 2007; Hoogewind et al., 2017; Li et al., 2021). These patterns, especially when contrasted with null-event days, exhibit larger maximum values and stronger gradients in WMAXSHEAR anomalies, as well as a closer spatial relationship between WMAXSHEAR and the lowest 500-hPa geopotential height anomalies (Fig. 2). This provides distinct thresholds that can be instrumental for analyzing future simulations.

Therefore, we suggest that the MCA patterns can be used as a proxy for characterizing the nature of tornado outbreaks in the simulations of future climate under various climate warming scenarios. The precise understanding of these patterns on tornado days, compared to their more diffuse signatures on null-event days, supports their potential as reliable indicators in climate modeling. Consequently, our results present a pathway to improved understanding of current and future tornado outbreak climatology and offer new avenues for improvements in tornado outbreak prediction based on pattern recognition.

This study has several limitations. First, to focus on the timing of peak occurrence of major tornado outbreaks, we constrained our data to the month of May. Other patterns might have been evident had we selected a different month. Second, we limited the analysis to one reanalysis dataset. Though ERA5 is commonly used for similar studies, its spatial resolution and period of record could influence the results as compared to other reanalyses (Coffer et al., 2020; Taszarek et al., 2021b). Third, the majority of tornadoes are rated EF0 or EF1, which means that many tornado outbreaks, particularly those dominated by weaker tornadoes, may not be fully represented in our analysis due to our focus on significant tornadoes (i.e., EF2 or greater). This focus might overlook some outbreak cases that consist primarily of weaker tornadoes, classified as null-events in our study, representing a limitation that should be considered when interpreting the results. Lastly, the complexity of the atmospheric systems involved poses a challenge. Although MCA found patterns using two anomaly fields known to relate to major tornado outbreaks, these fields are subsets of a broader, more intricate atmospheric framework. Specifically, changes in the 500-hPa geopotential height field are on much larger spatiotemporal scales than the mesoscale processes influencing the WMAXSHEAR field, which can change in a matter of hours. For that reason, the interplay between these scales introduces significant complexity, making it challenging to capture the full range of atmospheric interactions that lead to tornado outbreaks.

Upcoming work by the authors will examine the stationarity of these three patterns in the historical record, whether they are well represented in a global climate model, and how the frequency of these patterns changes (if at all) by the end of the century using climate projections. Additionally, future research could explore whether the large-scale atmospheric circulation patterns identified on outbreak days can also be detected on monthly timescales. While this is beyond the scope of the current study, it deserves further exploration to establish whether persistent, long-term atmospheric backgrounds are linked to major tornado outbreaks and how these connections might inform future research.

It is important to highlight that the use of MCA in this study is particularly unique. Typically, MCA is employed to explore relationships between large-scale climatic variables, such as sea surface temperature, and precipitation patterns (e.g., Salim et al., 2005; Barreto et al., 2017; Rieger et al., 2021). However, using MCA to analyze tornado outbreaks and to identify complex multivariate relationships between mid-atmospheric geopotential height anomalies and WMAXSHEAR anomalies is relatively new and innovative. This method provides a more nuanced spatial and temporal understanding of the atmospheric conditions that lead to tornado outbreaks, a topic that is not extensively covered in current literature. Employing MCA in this context addresses a significant gap in severe weather research and establishes a solid foundation for future studies to better predict and comprehend the effects of climate change on tornado activity. This enhanced understanding of tornado outbreak-related patterns and any associated changes in their frequency over time can ultimately improve societal preparedness for future weather hazards in a warming climate.

Open research

The US tornado reports were downloaded from the Storm Prediction Center Storm Data (https://www.spc.noaa.gov/wcm/data/1950-2022_actual_tornadoes.csv). The US state boundaries, used in mapping, are from the United States Census Bureau's 2017 Cartographic Boundary Files MAF/TIGER geographic database at the county level with 20-m (1:20000000) resolution (available at: https://www.census.gov/geographies/mapping-files/2017/geo/kml-cartographic-boundary-files.html, or alternatively at: https://www2.census.gov/geo/tiger/GENZ2017/kml/cb_2017_us_nation_20m.zip). The ERA5 Reanalysis data are provided by the European Centre for Medium-Range Weather Forecasts (ECMWF), Copernicus Climate Change Service (C3S) at Climate Data Store (CDS). For more details, refer to Hersbach et al. (2017). Raw ERA5 data was post-processed using the thundeR R language rawinsonde package available at: https://github.com/bczernecki/thundeR.

Author statement

The authors confirm their respective contributions to this study as follows:

1) Paulina Ćwik contributed to the conceptualization, data curation, formal analysis, investigation, methodology, validation, and visualization of the research. She also led the development and preparation of the original draft and revisions.

2) Jason Furtado contributed to the conceptualization and methodology, provided supervision, and contributed to the manuscript's review and editing.

3) Renee A. McPherson contributed to the conceptualization, funding acquisition, and resources for the project. She also provided supervision and contributed to the manuscript's review and editing.

4) Mateusz Taszarek contributed to data acquisition, curation and the manuscript's review and editing.

All authors have reviewed and approved the final manuscript.
Paulina Ćwik.

CRediT authorship contribution statement

Paulina Ćwik: Writing – review & editing, Writing – original draft, Visualization, Validation, Methodology, Investigation, Formal analysis, Conceptualization. **Jason C. Furtado:** Writing – review & editing, Validation, Supervision, Methodology. **Renee A. McPherson:** Writing – review & editing, Supervision, Funding acquisition, Conceptualization. **Mateusz Taszarek:** Writing – review & editing, Validation, Data curation.

Declaration of competing interest

The authors declare the following financial interests/personal relationships which may be considered as potential competing interests:

Paulina Cwik reports financial support was provided by The University of Oklahoma. Paulina Cwik reports a relationship with The University of Oklahoma that includes: employment. If there are other authors, they declare that they have no known competing financial interests or personal relationships that could have appeared to influence the work reported in this paper.

Data availability

Links to all data used in this work are available in the Open Research Section in the main manuscript.

Acknowledgments

Financial support for publication was provided by the University of Oklahoma Libraries' Open Access Fund. This research was supported by the South Central Climate Adaptation Science Center, the Office of the Vice President for Research, the Dean's Office of the College of Atmospheric and Geographic Sciences at the University of Oklahoma, and the Department of Geography and Environmental Sustainability at the University of Oklahoma. ERA5 data used in this work was post-processed with a thundeR package under the grant of the Polish National Science Center (no. 2020/39/D/ST10/00768).

Appendix A. Supplementary data

Supplementary data to this article can be found online at https://doi.org/10.1016/j.atmosres.2024.107872.

References

Allen, J.T., Allen, E.R., 2016. A review of severe thunderstorms in Australia. Atmos. Res. 178, 347–366. https://doi.org/10.1016/j.atmosres.2016.03.011.
Anderson-Frey, A.K., Brooks, H., 2021. Tornado fatalities: An environmental perspective. Weather Forecast. 34 (6), 1999–2015. https://doi.org/10.1175/WAF-D-19-0119.1.
Anderson-Frey, A.K., Richardson, Y.P., Dean, A.R., Thompson, R.L., Smith, B., 2016. Investigation of near-storm environments for tornado events and warnings. Weather Forecast. 31 (6), 1771–1790. https://doi.org/10.1175/WAF-D-16-0046.1.
Antonescu, B., Schultz, D.M., Holzer, A., Groenemeijer, P., 2017. Tornadoes in Europe: an underestimated threat. Bull. Am. Meteorol. Soc. 98 (4), 713–728. https://doi.org/10.1175/BAMS-D-16-0171.1.
Ashley, W.S., Haberlie, A.M., Gensini, V.A., 2023. The Future of Supercells in the United States. Bull. Am. Meteorol. Soc. 104 (1), E1–E21. https://doi.org/10.1175/BAMS-D-22-0027.1.
Bagaglini, L., Ingrosso, R., Miglietta, M.M., 2021. Synoptic patterns and mesoscale precursors of Italian tornadoes. Atmos. Res. 253, 105503. https://doi.org/10.1016/j.atmosres.2021.105503.
Barreto, N.J., Mesquita, M.D.S., Mendes, D., Spyrides, M.H., Pedra, G.U., Lucio, P.S., 2017. Maximum covariance analysis to identify intraseasonal oscillations over tropical Brazil. Clim. Dyn. 49, 1583–1596. https://doi.org/10.1007/s00382-016-3401-3.
Brooks, H.E., 2013. Severe Thunderstorms and Climate Change. Atmospheric Research. Elsevier. https://doi.org/10.1016/j.atmosres.2012.04.002.
Brooks, H.E., Lee, J.W., Craven, J.P., 2003a. The spatial distribution of severe thunderstorm and tornado environments from global reanalysis data. Atmos. Res. 67–68, 73–94. https://doi.org/10.1016/S0169-8095(03)00045-0.
Brooks, H., Doswell, C., Kay, M., 2003b. Climatological estimates of Local Daily Tornado Probability for the United States. Weather Forecast. 18 (4), 626–640. https://doi.org/10.1175/1520-0434(2003)018<0626:CEOLDT>2.0.CO;2.
Brown, M.C., Nowotarski, C.J., 2020. Southeastern U.S. Tornado Outbreak Likelihood using Daily climate Indices. J. Clim. 33 (8), 3229–3252. https://doi.org/10.1175/jcli-d-19-0684.1.
Chasteen, M.B., Koch, S.E., 2022. Multiscale aspects of the 26–27 April 2011 tornado outbreak. Part I: outbreak chronology and environmental evolution. Mon. Weather Rev. 150 (2), 309–335. https://doi.org/10.1175/MWR-D-21-0013.1.
Coffer, B.E., Parker, M.D., Thompson, R.L., Smith, B.T., Jewell, R.E., 2019. Using near-ground storm relative helicity in supercell tornado forecasting. Weather Forecast. 34 (5), 1417–1435. https://doi.org/10.1175/WAF-D-19-0115.1.
Coffer, B.E., Taszarek, M., Parker, M.D., 2020. Near-ground wind profiles of tornadic and nontornadic environments in the United States and Europe from ERA5 reanalyses. Weather Forecast. 35 (6), 2621–2638. https://doi.org/10.1175/WAF-D-20-0153.1.
Coniglio, M.C., Parker, M.D., 2020. Insights into supercells and their environments from three decades of targeted radiosonde observations. Mon. Weather Rev. 148 (12), 4893–4915. https://doi.org/10.1175/MWR-D-20-0105.1.
Corfidi, S.F., Weiss, S.J., Kain, J.S., Corfidi, S.J., Rabin, R.M., Levit, J.J., 2010. Revisiting the 3–4 April 1974 Super Outbreak of Tornadoes. Weather Forecast. 25 (2), 465–510. https://doi.org/10.1175/2009WAF2222297.1.

Ćwik, P., McPherson, R.A., Brooks, H.E., 2021. What is a Tornado Outbreak? Perspectives through Time. Bull. Am. Meteorol. Soc. 102 (4), E817–E835. https://doi.org/10.1175/BAMS-D-20-0076.1.
Ćwik, P., McPherson, R.A., Richman, M.B., Mercer, A.E., 2022. Climatology of 500-hPa geopotential height anomalies associated with May tornado outbreaks in the United States. Int. J. Climatol. 1–21. https://doi.org/10.1002/joc.7841.
Czernecki, B., Taszarek, M., Szuster, P., 2023. Thunder: Computation and Visualization of Atmospheric Convective Parameters. Retrieved from. https://bczernecki.github.io/thundeR/.
Davies-Jones, R., 2015. A review of supercell and tornado dynamics. Atmos. Res. 158, 274–291. https://doi.org/10.1016/j.atmosres.2014.04.007.
Diffenbaugh, N.S., Scherer, M., Trapp, R.J., 2013. Robust increases in severe thunderstorm environments in response to greenhouse forcing. Proc. Natl. Acad. Sci. 110 (41), 16361–16366. https://doi.org/10.1073/pnas.1307758110.
Doswell, C.A., Edwards, R., Thompson, R.L., Hart, J.A., Crosbie, K., 2006. A simple and flexible method for ranking severe weather events. Weather Forecast. 21 (6), 939–951. https://doi.org/10.1175/WAF959.1.
Edwards, R., Brooks, H.E., Cohn, H., 2021. Changes in Tornado Climatology Accompanying the Enhanced Fujita Scale. J. Appl. Meteorol. Climatol. 60 (10), 1465–1482. https://doi.org/10.1175/JAMC-D-21-0058.1.
Elsner, J.B., Michaels, L.E., Scheitlin, K.N., Elsner, I.J., 2013. The decreasing population bias in tornado reports across the Central Plains. Weather, Clim. Soc. 5 (4), 221–232. https://doi.org/10.1175/WCAS-D-12-00040.1.
Elsner, J.B., Elsner, S.C., Jagger, T.H., 2015. The increasing efficiency of tornado days in the United States. Clim. Dyn. 45 (3), 651–659. https://doi.org/10.1007/s00382-014-2277-3.
Fricker, T., Friesenhahn, C., 2022. Tornado fatalities in context: 1995–2018. Weather, Clim. Soc. 14 (1), 81–93. https://doi.org/10.1175/WCAS-D-21-0028.1.
Fuhrmann, C.M., Ii, C.E.K., Kovach, M.M., Mcleod, J.T., Schmitz, W.G., Dixon, P.G., 2014. Ranking of tornado outbreaks across the United States and their climatological characteristics. Weather Forecast. 29 (3), 684–701. https://doi.org/10.1175/WAF-D-13-00128.1.
Galway, J.G., 1977. Some Climatological Aspects of Tornado Outbreaks. Mon. Weather Rev. 105 (4), 477–484. https://doi.org/10.1175/1520-0493(1977)105<0477:SCAOTO>2.0.CO;2.
Gensini, V.A., Brooks, H.E., 2018. Spatial trends in United States tornado frequency. NPJ Clim. Atmosph. Sci. 1 (1), 38. https://doi.org/10.1038/s41612-018-0048-2.
Gensini, V.A., de Guenni, L.B., 2019. Environmental covariate representation of seasonal US tornado frequency. J. Appl. Meteorol. Climatol. 58 (6), 1353–1367. https://doi.org/10.1175/JAMC-D-18-0305.1.
Gensini, V.A., Mote, T.L., Brooks, H.E., 2014. Severe-thunderstorm reanalysis environments and collocated radiosonde observations. J. Appl. Meteorol. Climatol. 53 (3), 742–751. https://doi.org/10.1175/JAMC-D-13-0263.1.
Gensini, V.A., Gold, D., Allen, J.T., Barrett, B.S., 2019. Extended U.S. tornado outbreak during late May 2019: A forecast of opportunity. Geophys. Res. Lett. 46 (16), 10150–10158. https://doi.org/10.1029/2019GL084470.
Gilleland, E., 2020. Bootstrap methods for statistical inference. Part II: Extreme-value analysis. J. Atmos. Ocean. Technol. 37 (11), 2135–2144. https://doi.org/10.1175/JTECH-D-20-0070.1.
Groenemeijer, P., Kühne, T., 2014. A climatology of tornadoes in Europe: results from the European Severe Weather Database. Mon. Weather Rev. 142 (12), 4775–4790. https://doi.org/10.1175/MWR-D-14-00107.1.
Hartmann, D., 2016. Matrix Methods for Analysis of Structure in Data Sets. ATM 552 notes: Matrix *Methods*. EOF, SVD, pp. 68–110.
Hatzis, J.J., Koch, J., Brooks, H.E., 2020. A tornado daily impacts simulator for the central and southern United States. Meteorol. Appl. 27 (1), e1882. https://doi.org/10.1002/met.1882.
Hersbach, H., Bell, B., Berrisford, P., Hirahara, S., Horányi, A., Muñoz-Sabater, J., Nicolas, J., Peubey, C., Radu, R., Schepers, D., Simmons, A., Soci, C., Abdalla, S., Abellan, X., Balsamo, G., Bechtold, P., Biavati, G., Bidlot, J., Bonavita, M., De Chiara, G., Dahlgren, P., Dee, D., Diamantakis, M., Dragani, R., Flemming, J., Forbes, R., Fuentes, M., Geer, A., Haimberger, L., Healy, S., Hogan, R.J., Hólm, E., Janisková, M., Keeley, S., Laloyaux, P., Lopez, P., Lupu, C., Radnoti, G., de Rosnay, P., Rozum, I., Vamborg, F., Villaume, S., Thépaut, J-N., 2017. Complete ERA5 from 1940: Fifth generation of ECMWF atmospheric reanalyses of the global climate [Dataset]. Copernicus Climate Change Service (C3S) Data Store (CDS). Doi:10.24381/cds.143582cf.
Hersbach, H., Bell, B., Berrisford, P., Hirahara, S., Horányi, A., Muñoz-Sabater, J., et al., 2020. The ERA5 global reanalysis. Q. J. R. Meteorol. Soc. 146 (730), 1999–2049. https://doi.org/10.1002/qj.3803.
Hoogewind, K.A., Baldwin, M.E., Trapp, R.J., 2017. The impact of climate change on hazardous convective weather in the United States: Insight from high-resolution dynamical downscaling. J. Clim. 30 (24), 10081–10100. https://doi.org/10.1175/JCLI-D-16-0885.1.
Johns, R.H., Doswell III, C.A., 1992. Severe local storms forecasting. Wea. Forecasting 7 (4), 588–612. https://doi.org/10.1175/1520-0434(1992)007<0588:SLSF>2.0.CO;2.
King, A.T., Kennedy, A.D., 2019. North American supercell environments in atmospheric reanalyses and RUC-2. J. Appl. Meteorol. Climatol. 58 (1), 71–92. https://doi.org/10.1175/JAMC-D-18-0015.1.
Klockow, K.E., Peppler, R.A., McPherson, R.A., 2014. Tornado folk science in Alabama and Mississippi in the 27 April 2011 tornado outbreak. GeoJournal 79 (6), 791–804. https://doi.org/10.1007/s10708-013-9518-6.
Lee, C.C., 2012. Utilizing synoptic climatological methods to assess the impacts of climate change on future tornado-favorable environments. Nat. Hazards 62, 325–343. https://doi.org/10.1007/s11069-011-9998-y.
Lee, S.K., Atlas, R., Enfield, D., Wang, C., Liu, H., 2013. Is there an optimal ENSO pattern that enhances large-scale atmospheric processes conducive to tornado outbreaks in the United States? J. Clim. 26 (5), 1626–1642. https://doi.org/10.1175/JCLI-D-12-00128.1.
Li, F., D.R., C., Reed, K. A., Dawson, D. T., 2020. Climatology of severe local storm environments and synoptic-scale features over North America in ERA5 reanalysis and CAM6 simulation. J. Clim. 33 (19), 8339–8365. https://doi.org/10.1175/JCLI-D-19-0986.1.
Li, F., Chavas, D.R., Reed, K.A., Rosenbloom, N., Dawson II, D., 2021. The role of elevated terrain and the Gulf of Mexico in the production of severe local storm environments over North America. J. Clim. 34 (19), 7799–7819. https://doi.org/10.1175/JCLI-D-20-0607.1.
Marchand, R., Beagley, N., Thompson, S.E., Ackerman, T.P., Schultz, D.M., 2006. A bootstrap technique for testing the relationship between local-scale radar observations of cloud occurrence and large-scale atmospheric fields. J. Atmos. Sci. 63 (11), 2813–2830. https://doi.org/10.1175/JAS3772.1.
Markowski, P., Richardson, Y., 2010. Mesoscale Meteorology in Midlatitudes. John Wiley, Sons. https://doi.org/10.1002/9780470682104.
Marsh, P.T., Brooks, H.E., Karoly, D.J., 2007. Assessment of the severe weather environment in North America simulated by a global climate model. Atmos. Sci. Lett. 8 (4), 100–106. https://doi.org/10.1002/asl.159.
Masson-Delmotte, V.P., Zhai, P., Pirani, S.L., Connors, C., Péan, S., Berger, N., Caud, Y., Chen, L., Goldfarb, M.I., Scheel Monteiro, P.M., 2021. IPCC, 2021: Climate Change 2021: The Physical Science Basis (Contribution of Working Group I to the Sixth Assessment Report of the Intergovernmental Panel on Climate Change).
Mercer, A.E., Bates, A., 2019. Meteorological differences characterizing tornado outbreak forecasts of varying quality. Atmosphere 10 (1), 16. https://doi.org/10.3390/atmos10010016.
Mercer, A.E., Shafer, C.M., Doswell, C.A., Leslie, L.M., Richman, M.B., 2012. Synoptic Composites of Tornadic and Nontornadic Outbreaks. Mon. Weather Rev. 140 (8), 2590–2608. https://doi.org/10.1175/MWR-D-12-00029.1.
Molina, M.J., Allen, J.T., 2020. Regionally-stratified tornadoes: Moisture source physical reasoning and climate trends. Weather and Climate Extremes 28, 100244. https://doi.org/10.1016/j.wace.2020.100244.
Molina, M.J., Allen, J.T., Gensini, V.A., 2018. The Gulf of Mexico and ENSO influence on subseasonal and seasonal CONUS winter tornado variability. J. Appl. Meteorol. Climatol. 57 (10), 2439–2463. https://doi.org/10.1175/JAMC-D-18-0046.1.
Moore, T.W., DeBoer, T., 2019. A review and analysis of possible changes to the climatology of tornadoes in the United States. Progress Phys. Geograph.: Earth Environ. 43 (3), 365–390. https://doi.org/10.1080/24694452.2021.1910479.
Moore, T.W., Clair, J.M.S., McGuire, M.P., 2021. Climatology and Trends of Tornado-favorable Atmospheric Ingredients in the United States. Ann. Am. Assoc. Geogr. 1–19. https://doi.org/10.1080/24694452.2021.1910479.
Pilguj, N., Taszarek, M., Kryza, M., Brooks, H.E., 2022a. Reconstruction of violent tornado environments in Europe: High-resolution dynamical downscaling of ERA5. Geophys. Res. Lett. 49 (11). https://doi.org/10.1029/2022GL098242 e2022GL098242.
Pilguj, N., Taszarek, M., Allen, J.T., Hoogewind, K.A., 2022b. Are trends in convective parameters over the United States and Europe consistent between reanalyses and observations? J. Clim. 35 (12), 3605–3626. https://doi.org/10.1175/JCLI-D-21-0135.1.
Prohaska, J.T., 1976. A Technique for Analyzing the Linear Relationships between two Meteorological Fields. Mon. Weather Rev. 104 (11), 1345–1353. https://doi.org/10.1175/1520-0493(1976)104<1345:ATFATL>2.0.CO;2.
Púčik, T., Rýva, D., Staněk, M., Šinger, M., Groenemeijer, P., Pistotnik, G., Kaltenberger, R., Zich, M., Koláček, J., Holzer, A., 2024. The violent tornado on 24 June 2021 in Czechia: damage survey, societal impacts and lessons learned. Weather, Clim. Soc. https://doi.org/10.1175/WCAS-D-23-0080.1.
Rasmussen, E.N., 2003. Refined supercell and tornado forecast parameters. Weather Forecast. 18 (3), 530–535. https://doi.org/10.1175/1520-0434(2003)18<530:RSATFP>2.0.CO;2.
Rasmussen, E.N., Blanchard, D.O., 1998. A baseline climatology of sounding-derived supercell and tornado forecast parameters. Weather Forecast. 13 (4), 1148–1164. https://doi.org/10.1175/1520-0434(1998)013<1148:ABCOSD>2.0.CO;2.
Rieger, N., Corral, Á., Olmedo, E., Turiel, A., 2021. Lagged teleconnections of climate variables identified via complex rotated maximum covariance analysis. J. Clim. 34 (24), 9861–9878. https://doi.org/10.1175/JCLI-D-21-0244.1.
Roebber, P.J., Schultz, D.M., Romero, R., 2002. Synoptic regulation of the 3 May 1999 tornado outbreak. Weather Forecast. 17 (3), 399–429. https://doi.org/10.1175/1520-0434(2002)017<0399:SROTMT>2.0.CO;2.
Rothfusz, L.P., Schneider, R., Novak, D., Klockow-McClain, K., Gerard, A.E., Karstens, C., Strumpf, G.J., Smith, T.M., 2018. FACETs: A proposed next-generation paradigm for high-impact weather forecasting. Bull. Am. Meteorol. Soc. 99 (10), 2025–2043. https://doi.org/10.1175/BAMS-D-16-0100.1.
Salim, A., Pawitan, Y., Bond, K., 2005. Modelling association between two irregularly observed spatiotemporal processes by using maximum covariance analysis. J. R. Stat. Soc.: Ser. C: Appl. Stat. 54 (3), 555–573. https://doi.org/10.1111/j.1467-9876.2005.05300.x.
Schaefer, J.T., Edwards, R., 1999. The SPC tornado/severe thunderstorm database. In: Preprints, 11th Conf. on Applied Climatology, 6. Amer. Meteor. Soc, Dallas, TX.
Schroder, Z., Elsner, J.B., 2020. Quantifying relationships between environmental factors and power dissipation on the most prolific days in the largest tornado “outbreaks.”. Int. J. Climatol. 40 (6), 3150–3160. https://doi.org/10.1002/joc.6388.
Shafer, C.M., Doswell, C.A., 2011. Using kernel density estimation to identify, rank, and classify severe weather outbreak events. Electronic J. Severe Storms Meteorol. 6 (2), 1–28. https://www.researchgate.net/publication/271196631.

Sherburn, K.D., Parker, M.D., 2014. Climatology and Ingredients of significant Severe Convection in High-Shear, Low-CAPE Environments. Weather Forecasting 29 (4), 854–877. https://doi.org/10.1175/WAF-D-13-00041.1.

Silverman, B.W., 1986. Density Estimation for Statistics and Data Analysis, vol. 26. CRC press.

Simmons, K.M., Sutter, D., Pielke, R., 2013. Normalized tornado damage in the United States: 1950–2011. Environ. Hazards 12 (2), 132–147. https://doi.org/10.1080/17477891.2012.738642.

Sparrow, K.H., Mercer, A.E., 2016. Predictability of US tornado outbreak seasons using ENSO and northern hemisphere geopotential height variability. Geosci. Front. 7 (1), 21–31. https://doi.org/10.1016/j.gsf.2015.07.007.

Stendel, M., Francis, J., White, R., Williams, P.D., Woollings, T., 2021. The jet stream and climate change. Elsevier, Climate change 327-357. https://doi.org/10.1016/B978-0-12-821575-3.00015-3.

Strader, S.M., Pingel, T.J., Ashley, W.S., 2016. A Monte Carlo model for estimating tornado impacts. Meteorol. Appl. 23 (2), 269–281. https://doi.org/10.1002/met.1552.

Strader, S.M., Ashley, W.S., Pingel, T.J., Krmenec, A.J., 2017. Observed and projected changes in United States tornado exposure. Weather, Clim. Soc. 9 (2), 109–123. https://doi.org/10.1175/WCAS-D-16-0041.1.

Sutter, D., Simmons, K.M., 2010. Tornado fatalities and mobile homes in the United States. Nat. Hazards 53, 125–137. https://doi.org/10.1007/s11069-009-9416-x.

Taszarek, Mateusz, Allen, J.T., Púčik, T., Hoogewind, K.A., Brooks, H.E., 2020. Severe Convective Storms across Europe and the United States. Part II: ERA5 Environments Associated with Lightning, large Hail, Severe Wind, and Tornadoes. J. Clim. 33 (23), 10263–10286. https://doi.org/10.1175/JCLI-D-20-0346.1.

Taszarek, Mateusz, Allen, J.T., Brooks, H.E., Pilguj, N., Czernecki, B., 2021a. Differing trends in United States and European severe thunderstorm environments in a warming climate. Bull. Am. Meteorol. Soc. 102 (2), E296–E322. https://doi.org/10.1175/BAMS-D-20-0004.1.

Taszarek, M., Pilguj, N., Allen, J.T., Gensini, V.A., Brooks, H.E., Szuster, P., 2021b. Comparison of convective parameters derived from ERA5 and MERRA-2 with rawinsonde data over Europe and North America. J. Clim. 34 (8), 211–3237. https://doi.org/10.1175/JCLI-D-20-0484.1.

Taszarek, Mateusz, Czernecki, B., Szuster, P., 2023. ThundeR - a rawinsonde package for processing convective parameters and visualizing atmospheric profiles. In: In 11th European Conference on Severe Storms. Bucharest, Romania. https://doi.org/10.5194/ecss2023-28. Retrieved from.

Thompson, R.L., Edwards, R., Hart, J.A., Elmore, K.L., Markowski, P., 2003. Close proximity soundings within supercell environments obtained from the Rapid Update Cycle. Weather Forecast. 18 (6), 1243–1261. https://doi.org/10.1175/1520-0434(2003)018<1243:CPSWSE>2.0.CO;2.

Thompson, R.L., Edwards, R., Mead, C.M., 2004. An update to the supercell composite and significant tornado parameters. In: Preprints, 22nd Conf. On Severe Local Storms, vol. 8. Amer. Meteor. Soc, Hyannis, MA, p. P8.1.

Thompson, R.L., Smith, B.T., Grams, J.S., Dean, A.R., Broyles, C., 2012. Convective Modes for significant Severe Thunderstorms in the Contiguous United States. Part II: Supercell and QLCS Tornado Environments. Weather Forecast. 27 (5), 1136–1154. https://doi.org/10.1175/WAF-D-11-00116.1.

Tippett, M.K., 2014. Changing volatility of U.S. annual tornado reports. Geophys. Res. Lett. 41 (19), 6956–6961. https://doi.org/10.1002/2014GL061347.

Tippett, M.K., Lepore, C., Cohen, J.E., 2016. More tornadoes in the most extreme U.S. tornado outbreaks. Science 354 (6318), 1419–1423. https://doi.org/10.1126/science.aah7393.

Tochimoto, E., Niino, H., 2016. Structural and environmental characteristics of extratropical cyclones that cause tornado outbreaks in the warm sector: A composite study. Mon. Weather Rev. 144 (3), 945–969. https://doi.org/10.1175/MWR-D-15-0015.1.

Trapp, R.J., Hoogewind, K.A., 2016. The realization of extreme tornadic storm events under future anthropogenic climate change. J. Clim. 29 (14), 5251–5265. https://doi.org/10.1175/JCLI-D-15-0623.1.

Trapp, R., Diffenbaugh, N., Brooks, H., Baldwin, M., Robinson, E., Pal, J., 2007. Changes in severe thunderstorm environment frequency during the 21st century caused by anthropogenically enhanced global radiative forcing. In: Proceedings of the National Academy of Sciences, 104(50), pp. 19719–19723. https://doi.org/10.1073/pnas.0705494104.

Trapp, R., Diffenbaugh, N., Gluhovsky, A., 2009. Transient response of severe thunderstorm forcing to elevated greenhouse gas concentrations. Geophys. Res. Lett. 36 (1). https://doi.org/10.1029/2008GL036203.

Wilks, D.S., 2011. Statistical Methods in the Atmospheric Sciences, vol. 100. Academic Pres.